RESOLUTION OF ESTIMATED SOURCE PROCESS DEPENDING ON THE BACKWARD INFORMATION INVESTIGATED BY MULTI-SCALE INVERSION METHOD

Y. Ishii[1], H. Goto[2] and S. Sawada[3]

[1] *Institute of Technology, Shimizu Corporation, Tokyo, Japan*
[2] *Assistant Professor, Disaster Prevention Research Institute, Kyoto University, Kyoto, Japan*
[3] *Professor, Disaster Prevention Research Institute, Kyoto University, Kyoto, Japan*
Email: yayoi.ishii@shimz.co.jp, goto@catfish.dpri.kyoto-u.ac.jp, sawada@catfish.dpri.kyoto-u.ac.jp

ABSTRACT :

An element refinement algorithm based on sensitivity analysis is proposed and applied to kinematic source inversion analysis. The high sensitivity element on a target fault, which is selected by calculating the Hessian matrix of objective function for the inversion analysis, is divided into two small elements. Optimal element layout based on the sensitivity is obtained by recurring the dividing steps. Numerical examples show that the resolution of slip distributions in the inversion analysis depends on the arrangement of observation sites. It is also found that decreasing the residual between the observed and synthetic waveforms does not always mean improving the estimation of slip distribution.

KEYWORDS: source process, kinematic source inversion, element refinement

1. INTRODUCTION

Source rupture processes in generating strong ground motions have been investigated by using a kinematic source inversion method during major historical earthquakes. The rupture processes investigated, which consist of time and space distributions of slips on the fault, are empirically characterized in order to estimate ground motions during future earthquakes (e.g. Somerville *et al*., 1999, Irikura and Miyake, 2001, Dan *et al*., 2001). The estimated ground motions are applied to seismic designs of important infrastructures, nuclear power plants, etc. on the basis of the performance-based design.

However, the slip distributions obtained by the source inversion analyses are not proved an appropriate solution under the given conditions. For example, Mai *et al*. (2007) reported a summary of blind test which gives waveform data on the free surface and the exact model of subsurface structure. The results estimated by several researchers vary a lot from the true distributions.

Fine mesh layout, which consists of smaller size of elements, gives a smaller fluctuation of a slip distribution than coarse mesh layout, whereas the fluctuation does not always represent a true slip. In other words, the layout of element is required to match with a resolution based on arrangement of observation sites, geometry of faults, subsurface structures and reliable frequency bands. A non-uniform element layout according to the resolutions may give an appropriate solution under the given condition because the resolution should not be uniform over the fault. In this study, we propose an element refinement algorithm by finding a high sensitivity element in order to discuss the resolution of the estimated slip distributions and to evaluate the optimum non-uniform layout of the elements.

2. ELEMENT REFINEMENT ALGORITHM

2.1. Kinematic Source Inversion

Ground motion due to a displacement across the fault surface is expressed as the convolution of the Green's function and moment density tensor corresponding to the slip distribution on the fault surface, which is called representation theorem (Aki and Richards, 2000)). Hartzell and Heaton (1983) descretized the integral representation theorem is

space. The ground motion is expressed by a summation of the product of synthetic waveforms from each small element with a weight of element slip as.

$$\boldsymbol{d} = \boldsymbol{G}\boldsymbol{m} = \sum_{k=1}^{n} \boldsymbol{G}_k m_k , \tag{2.1}$$

where $\boldsymbol{d}$ is a vector of the ground motion, $\boldsymbol{G}$ a matrix of the Green's function, $\boldsymbol{m}$ a vector of the slips at the elements, $\boldsymbol{G_k}$ a vector of the Green's function for the kth element and m_k the slip at the kth element. Eqn. 2.1 is called "observation equation".

Kinematic source inversion method estimates the slip distribution on the fault from the observed ground motions. Its optimal solution is obtained by minimizing the difference between the observed and synthetic waveforms which are calculated by Eqn. 2.1. The objective function used for the inversion method is expressed by Eqn. 2.2.

$$J = \frac{1}{2}\left(\hat{\boldsymbol{d}} - \boldsymbol{G}\boldsymbol{m}\right)^T \left(\hat{\boldsymbol{d}} - \boldsymbol{G}\boldsymbol{m}\right) \rightarrow \min . \tag{2.2}$$

where $\hat{\boldsymbol{d}}$ is a vector of the observed ground motion.

2.2. Element Refinement

The optimal solutions of Eqn. 2.2 depend on a mesh layout of elements, which is related to the descretization of the integral representation theorem. In the conventional inversion method, the layout is regarded as a preliminary condition. In order to find appropriate layout and sizes of elements, we propose a strategy to divide inappropriate size of elements.

When the lth element is divided into 2 elements, Eqn. 2.1 is rewritten as

$$\begin{aligned} \boldsymbol{d} &= \sum_{k \neq l}^{n} \boldsymbol{G}_k m_k + \boldsymbol{G}_l m_l \\ &= \sum_{k \neq l}^{n} \boldsymbol{G}_k m_k + \boldsymbol{G}_l^{(1)} m_l^{(1)} + \boldsymbol{G}_l^{(2)} m_l^{(2)} , \end{aligned} \tag{2.3}$$

where $m_l^{(1)}$ and $m_l^{(2)}$ are the slips at the divided lth elements. $\boldsymbol{G}_l^{(1)}$ and $\boldsymbol{G}_l^{(2)}$ are vectors of Green's function for the divided lth elements. Eqn. 2.3 can be rewritten as follows.

$$\begin{aligned} \mathbf{d} &= \sum_{k=1}^{l-1} \tilde{\mathbf{G}}_k \tilde{m}_k + \tilde{\mathbf{G}}_l \tilde{m}_l + \tilde{\mathbf{G}}_{n+1} \tilde{m}_{n+1} + \sum_{k=l+1}^{n} \tilde{\mathbf{G}}_k \tilde{m}_k \\ &= \sum_{k=1}^{n+1} \tilde{\mathbf{G}}_k \tilde{m}_k \end{aligned} \tag{2.4}$$

$$\begin{cases} \tilde{\mathbf{G}}_k = \mathbf{G}_k & \tilde{m}_k = m_k \\ \tilde{\mathbf{G}}_l = \mathbf{G}_l^{(1)} & \tilde{m}_l = m_l^{(1)} \\ \tilde{\mathbf{G}}_{n+1} = \mathbf{G}_l^{(2)} & \tilde{m}_{n+1} = m_l^{(2)} \end{cases} \quad \text{for } k \neq l, k \leq n$$

Note that Eqn. 2.4 is the same structure with Eqn. 2.1, while the number of summations is different. We can treat all elements with different sizes, resulted by the dividing process mentioned below, based on the same structure of the observation equation.

2.3. Selection Criteria for Dividing Element

To make a criterion for selecting element divided, we focused on the objective function Eqn. 2.2. Optimal slip vector $\boldsymbol{m}^*$ of Eqn. 2.4 satisfies the following equation;

$$\nabla J = \boldsymbol{G}^T\left(\boldsymbol{d} - \boldsymbol{G}\boldsymbol{m}^*\right) = 0. \tag{2.5}$$

The difference of ∇J caused by a variation of $\boldsymbol{m}$ with the unit quantity is proportional to $\boldsymbol{G}^T\boldsymbol{G}$ which is the Hessian matrix of J. The high sensitivity element, which should be divided at the next step, is defined as the element giving the largest value of the diagonal components of $\boldsymbol{G}^T\boldsymbol{G}$ for the sake of simplicity. A new layout of elements at the next step is given by dividing the high sensitivity element. By applying the dividing processes recursively, the division of elements is optimized on the basis of the sensitivity.

3. NUMERICAL TEST

To confirm the validity of the proposed element refinement algorithm, three cases of the inversion analyses are performed. We assume a line source with 320 m length embedded in 2-D P-SV wave field (Fig. 1). P-wave velocity, S-wave velocity and density are assumed 6000m/sec, 3464m/sec and 2670kg/m^3, respectively. Synthetic waveforms are calculated for 3 cases with different arrangement of observation sites. Case-a (Fig. 1 (a)) consists of 3 observation sites on the free surface above the fault. One of them is located just above the center of the fault and the others are located 400m away from the center to right and left directions. Case-b (Fig. 1 (b)) consists of 4 sites; 3 sites in Case-a and the other site which is located 200m away from the center to right direction. Case-c (Fig. 1 (c)) consists of 4 sites; 3 sites in Case-a and the other site located 200m away from the center to left direction.

Figure 2 shows the given slip distribution to calculate the "observed" waveform for the inversion analysis. The star mark shows the location of hypocenter. Rupture mainly propagates in right direction, which is recognized as a unilateral rupture. It is noticed that Case-b has an additional site located in the forward direction of the rupture and Case-c has an additional site located in the backward direction. The slip time history consists of a smoothed ramp function with 0.1 sec of rise time. We set the rupture velocity 2770 m/s. Theoretical Green's functions are calculated by FE analysis, which models an area of 2000m width and 1000m depth with 10m of the node intervals. The calculated duration is 1.0 seconds with 0.001 seconds of the time interval.

Two elements of 160m widths are set at the initial step (Step 1). In the following steps, a high sensitivity element is divided into two. In Step 2, for example, two elements of 80m widths and one element of 160m are considered. In this paper, the dividing process is recurred until all elements become 40m widths, in order to check the variation of estimated slip distributions. The "observed" and calculated waveforms, which are re-sampled with 0.005 sec of time increment, are compared in the time window with 0.6 seconds length.

The estimated slip distributions of each step are shown in Fig. 3. The fault is divided into four elements of 80m widths at Step3 and eight elements of 40m at Step7. It means that the estimated slips at Step3 and Step7 are equivalent to the conventional kinematic source inversion, in which all elements have a uniform size. Figure 4 shows the comparisons between the "observed" waveforms and synthetic ones, which are calculated from the slip distribution estimated by the inversion analysis. Figure 5 also shows the estimation error of slip distributions e_{slip} and the estimation error of waveforms e_{wave}, defined by the following equations.

$$e_{slip} = \left\|\boldsymbol{m}_0 - \boldsymbol{m}\right\|^2, \tag{2.6}$$

$$e_{wave} = \left\|\boldsymbol{d} - \boldsymbol{G}\boldsymbol{m}\right\|^2, \tag{2.7}$$

where $\boldsymbol{m}_0$ is vector of the given slip distribution.

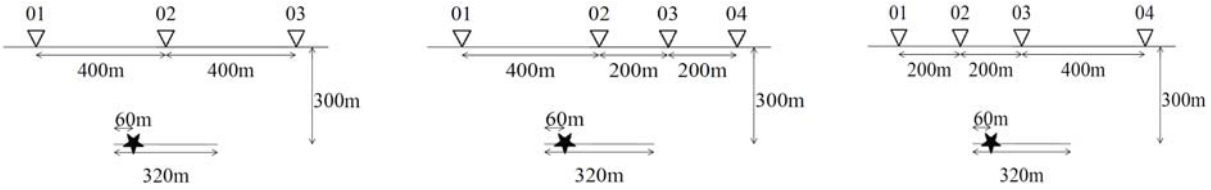

(a) Case-a (b) Case-b (c) Case-c

Figure 1 Locations of fault, hypocenter and observation sites

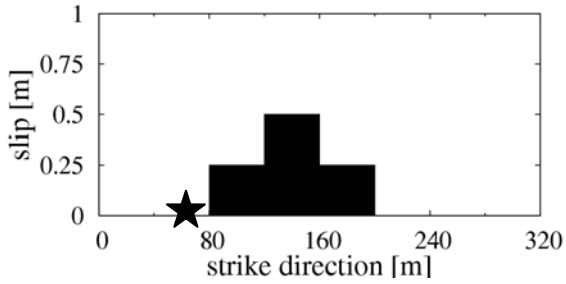

Figure 2 Given slip distribution

2.3.1 Results of Case-a (3 sites)

At Step 2 the estimation error of slip distributions and the estimation error of waveforms decrease much. At Step 3 the estimation error of slip distributions decreases while the estimation error of waveforms remains. Although the number of elements increases from Steps 4 to 5, the errors are almost constant. At Steps 6 and 7, the estimation error of waveforms decreases, while the estimation error of slip distributions increases. Decreasing the estimation error of waveforms does not always means improving slip distribution. It should be because the given condition has no enough resolution to divide the elements at Steps 6 and 7. In Case-a the estimated slip distribution at Step 5 is recognized as the optimum solution under the given condition.

2.3.2 Results of Case-b (4 sites: with additional site in forward direction)

Both errors decrease at Steps 2 and 3, while these remain at Step 4 because the slip distribution is not changed by the division. At Steps 5 and 6 the estimation error of waveforms decreases while the estimation error of slip distributions increases much. It may be beyond the resolution at these steps. However, the optimum solution is not distinguished in this case because both errors decrease at Step 7.

2.3.3 Results of Case-c (4 sites: with additional site in backward direction)

As the number of elements increase at each step, both errors decrease. This implies that the estimated slip distribution at Step 7 is the optimum solution under the given condition. It means that the arrangement of observation sites in Case-c, which includes an additional site in the backward direction, has higher resolution than Case-a and Case-b.

3. CONCLUSIONS

Element refinement algorithm based on the sensitivity analysis is proposed. The high sensitivity element, which gives the maximum value of the diagonal components of Hessian matrix at a step, is divided into two small elements at the next step. The dividing steps recur in order to obtain an optimal element layout based on the sensitivity. We apply the proposed algorithm to the kinematic source inversion analysis. The numerical examples show that the resolution of the source inversion analysis depends on the arrangement of observation sites; the case including an additional site to the rupture backward direction has the highest resolution among the examples.

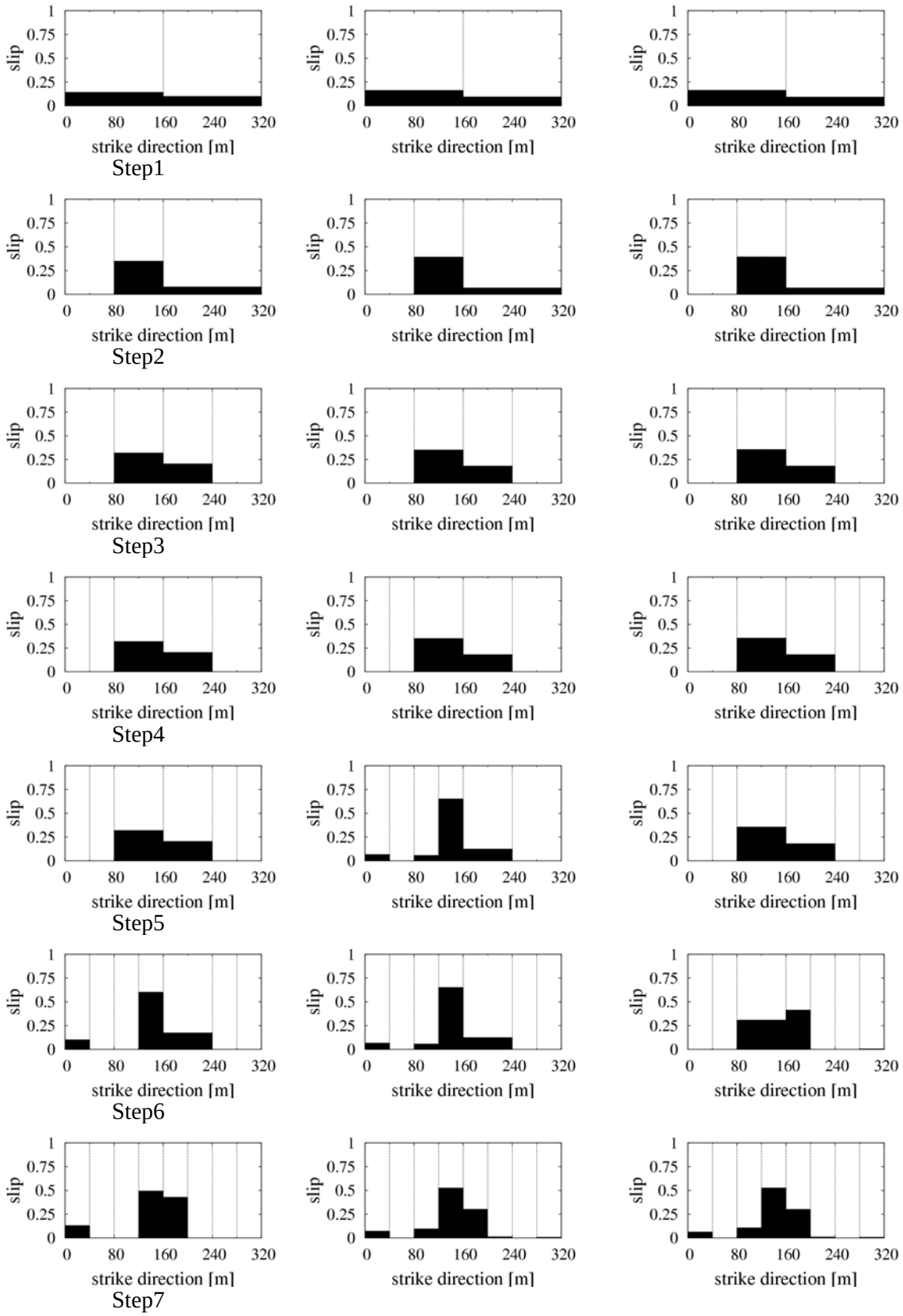

(a) Case-a (b) Case-b (c) Case-c

Figure 3 Estimated slip distributions

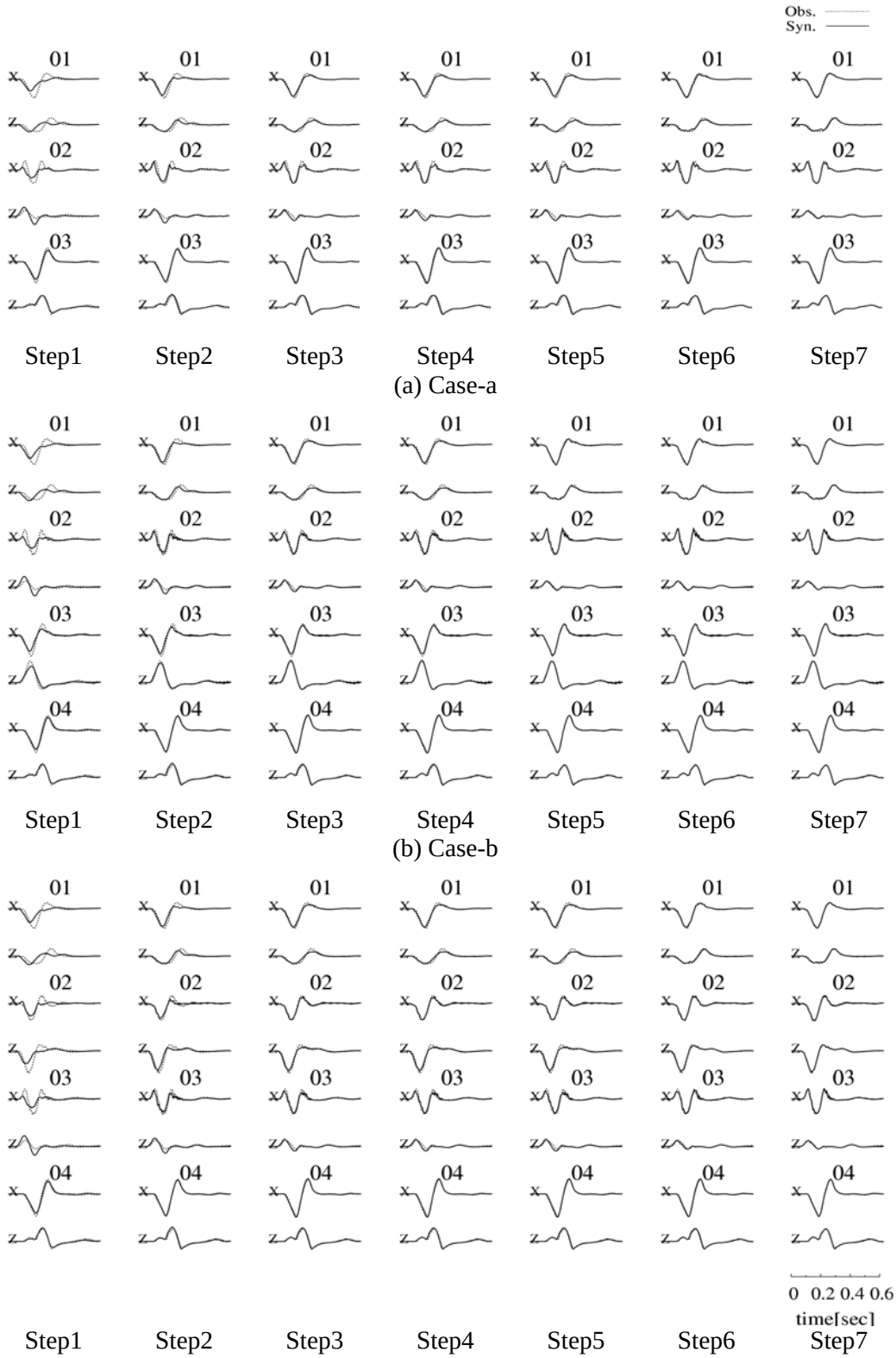

(a) Case-a

(b) Case-b

(c) Case-c

Figure 4 Comparison between the observed and synthetic waveforms

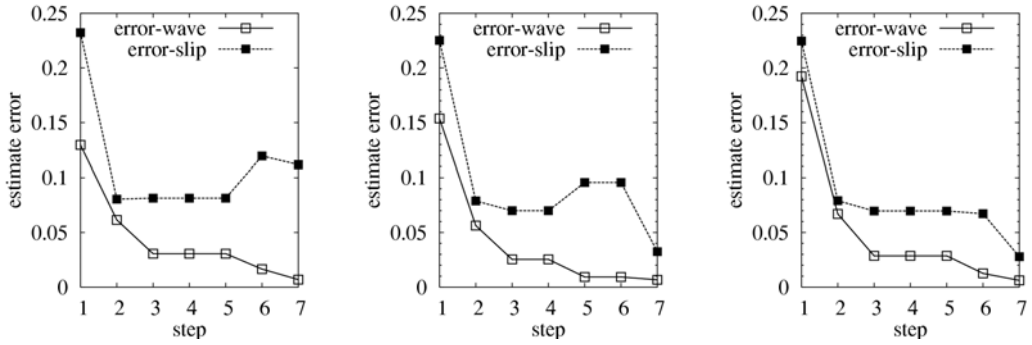

(a) Case-a (b) Case-b (c) Case-c

Figure 5 Estimation errors of each step

REFERENCES

Aki, K. and Richards, P. G. (2000), Quantitative Seismology Second Edition, University Science Books.

Dan, K., Watanabe, M., Sato, T. and Ishii, T. (2001). Short-period source spectra inferred from variable-slip rupture models and modeling of earthquake faults for strong motion prediction by semi-empirical method, *J*ournal *of Structural and* Construction Engineering, *AIJ*, **545**, 51-62 (in Japanese).

Hartzell, S.H. and Heaton, T.H. (1983). Inversion of strong ground motion and teleseismic waveform data for the fault rupture history of the 1979 Imperial Valley, California, earthquake, *Bulletin of the Seismological Society of America*, **73:6**, 1553-1583.

Irikura, K. and Miyake, H. (2001). Prediction of strong ground motions for scenario earthquakes, *Jounal of Geography*, **110:6,** 849-875.

Mai, M. P., Burjanek, J., Delouis, B., Festa, G., Francois-Holden, C., Monelli, D., Uchide, T. and Zahradnik, J. (2007). Earthquake source inversion blind test: Initial results and further developments, *Eos Trans. AGU, 88(52), Fall Meet. Suppl.*, Abstract S53C-08.

Somerville, P. G., Irikura, K., Graves, R., Sawada, S., Wald, D., Abrahamson, N., Iwasaki, Y., Kagawa, T., Smith, N. and Kowada, A. (1999). Characterizing crustal earthquake slip models for the prediction of strong ground motion, *Seismological Research Letters*, **70:1**, 59-80.